

Assessing the potential of Ge/SiGe quantum dots as hosts for singlet-triplet qubits

A. Hofmann,^{*,†,¶} D. Jirovec,^{*,†,¶} M. Borovkov,[†] I. Prieto,[†] A. Ballabio,[‡] J. Frigerio,[‡] D. Chrastina,[‡] G. Isella,[‡] and G. Katsaros[†]

[†]*IST Austria, Am Campus 1, 3400 Klosterneuburg*

[‡]*L-NESS, Department of Physics, Politecnico di Milano, Via Anzani 42, 22100 Como, Italy*

[¶]*Contributed equally*

E-mail: andrea.hofmann@ist.ac.at; daniel.jirovec@ist.ac.at

Abstract

We study double quantum dots in a Ge/SiGe heterostructure and test their maturity towards singlet-triplet ($S-T_0$) qubits. We demonstrate a large range of tunability, from two single quantum dots to a double quantum dot. We measure Pauli spin blockade and study the anisotropy of the g -factor. We use an adjacent quantum dot for sensing charge transitions in the double quantum dot at interest. In conclusion, Ge/SiGe possesses all ingredients necessary for building a singlet-triplet qubit.

Introduction

Germanium has turned out to be a versatile material for the study of physics at the nanoscale. Confinement into lower dimensions has been achieved in the form of epitaxially grown Ge/Si core/shell nanowires¹⁻⁶ as well as in dome-islands^{7,8} and hut-wires⁹⁻¹⁴ by controlling the assembly of Ge on Si. Holes are confined in the Ge-rich part of these nanostructure, thus

enabling low-dimensional p-type transport. Using appropriate gate-layouts, fully confined valence band states have been used for semiconductor spin qubits with record manipulation time.¹¹

In a different approach, building a Ge quantum well (QW) by sandwiching it with SiGe barriers has shown to yield high mobilities of $\mu = 1.1 \times 10^6 \text{ cm}^2/\text{Vs}$ at a density $p = 3 \times 10^{11} \text{ cm}^{-2}$ when modulation doping it with boron atoms.¹⁵ Even though the mobility is lower in undoped Ge/SiGe heterostructures¹⁶ ($\mu = 5 \times 10^5 \text{ cm}^2/\text{Vs}$ at $p = 6 \times 10^{11} \text{ cm}^{-2}$), the absence of dopands promises a reduction in scattering and charge noise,¹⁷ which will be important for building quantum-dot based qubits.^{18–21} Concerning such, recent studies^{22–24} show that the large spin–orbit interaction allows for 100 MHz Rabi frequencies in spin-qubits and two-qubit logic, and that the low effective mass ($\approx 0.05 m_e$ at low density²²) features sizable orbital energy spacings. Additionally, low hyperfine interaction^{25,26} inherent for holes in general and heavy-holes²⁵ hosted in nuclear-spin-free material in particular promises a quiet qubit environment.

Here, we take a closer look various other ingredients which will be necessary for further studies of (qubits in) undoped Ge/SiGe heterostructures, in particular towards the realization of singlet-triplet qubits (S - T_0 -qubits).^{27,28} An S - T_0 -qubit takes as a basis the singlet and unpolarized triplet states formed by two electron spins each of which sits in one of two coupled single quantum dots (SQDs). These two states are separated in energy by the exchange interaction, which in turn is a function of the detuning ϵ and the tunnel coupling t . The Rabi oscillation is caused by the energy difference between their symmetric and anti-symmetric superposition. In the absence of hyperfine interaction,²⁹ this energy difference is dominated by the difference in the g -factors in the left and right SQD.³⁰ With the large spin–orbit interaction of valence band states in Ge allowing for electrical tunability of the g -factor,^{31,32} an S - T_0 -qubit will be an interesting alternative to the Loss-DiVincenzo spin qubit.¹⁸ In this respect, our interest in the present work lies in analyzing the following parameters of Ge quantum dots,³³ which will be important for a S - T_0 -qubit: the tunability

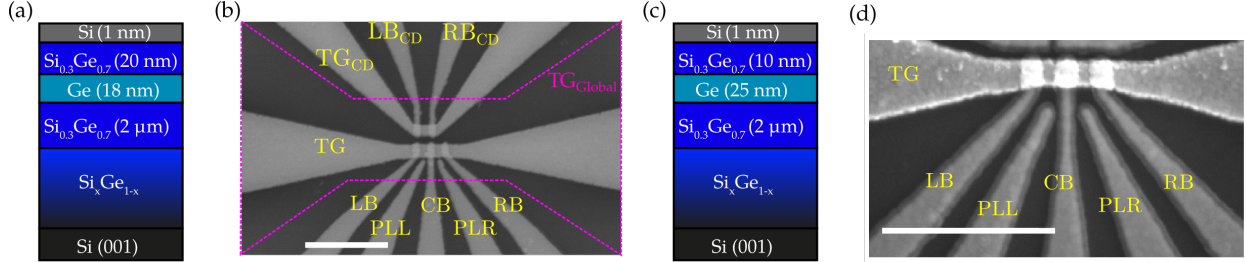


Figure 1: Sample overview. Panels (a-b) describe sample **A** and panels (c-d) describe sample **B**. Panels (a,c) display the growth layer stack. Both heterostructures have been grown using low energy plasma enhanced chemical vapor deposition. Standard silicon nanofabrication techniques have been used to fabricate the devices shown in panels (b,d). The scale-bar indicates 1 μm . Gates labeled TG are used as accumulation gates and lie on top of the other gates, with a layer of aluminium oxide in-between. The lower level of gates are used in depletion mode and function as barriers.

of the inter-dot tunnel coupling, the presence of Pauli spin blockade (PSB), charge readout with a capacitively coupled sensor and the g -factor anisotropy.

Results and discussion

Tunable double quantum dots

We present results from two samples originating from two different heterostructures, but similar top-gate layout. The relevant information about sample **A** and **B** are summarized in Fig. 1(a-b) and (c-d), respectively. The active layer in each heterostructure consists of a strained Ge QW confined between two strain-relaxed Si_{0.3}Ge_{0.7} barrier layers, as shown schematically in Fig. 1(a,c). This material combination provides an insulating state in equilibrium at cryogenic temperatures but hosts a two-dimensional hole gas (2DHG) once the Fermi energy is tuned into the valence band, for example by applying a negative voltage to a metallic top-gate electrode. The 2DHG of sample **A** is characterized by a mobility of $\mu = 26\,000\text{ cm}^2/\text{Vs}$ at a density of $p = 1.1 \times 10^{12}\text{ cm}^{-2}$ as measured at 4 K. The samples are grown using low energy plasma enhanced chemical vapor deposition.³⁴ In Fig. 1(b,d), the accumulation gates indicated as TG and TG_{CD} serve to accumulate charges in the 2DHG,

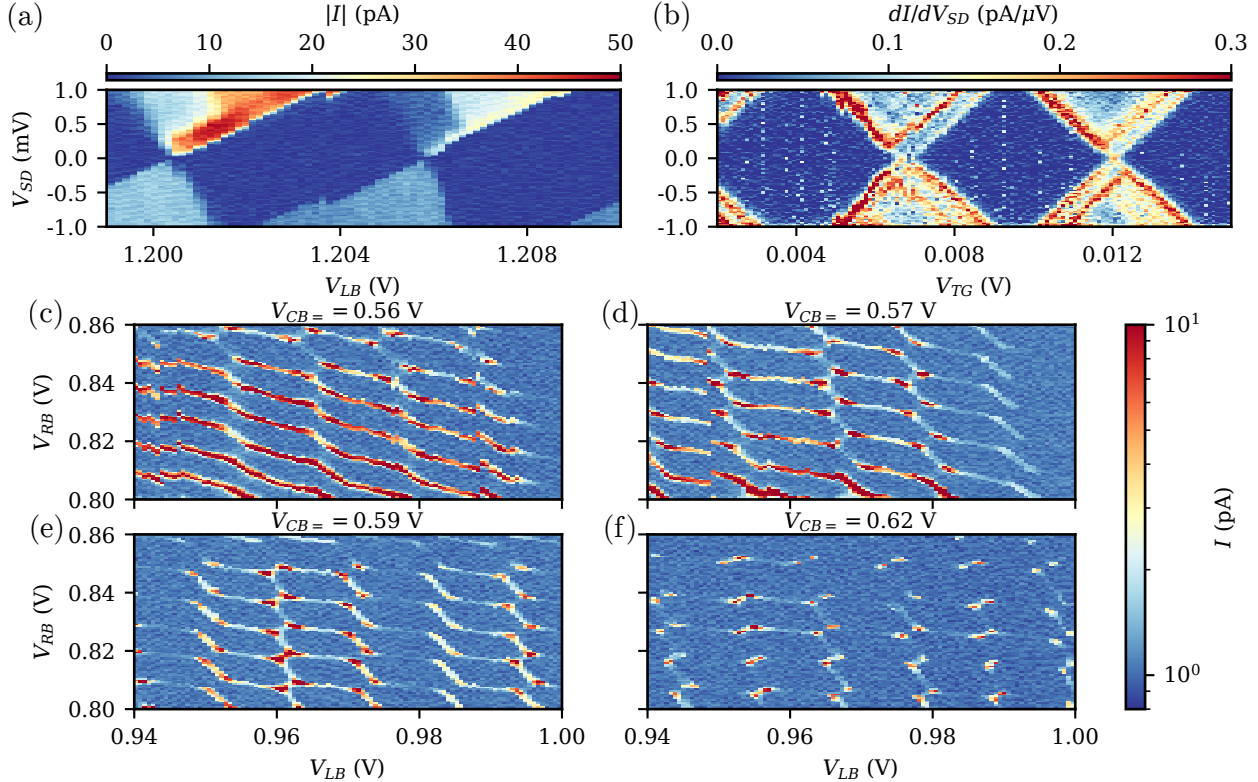


Figure 2: Tunability of Ge/SiGe quantum dots. Panels (a) and (b) each display Coulomb diamonds measured in a SQD formed by using, respectively, the left and right set of gates in sample **B**. Turning on both dots simultaneously, we form a double quantum dot (DQD) shown in panels (c-f). The gate CB controls the tunnel coupling between the two dots, allowing for a tunability ranging from a quantum dot molecule to a DQD formed by two isolated SQDs.

while the finger gates located below the accumulation gates locally screen their electric field and function as barrier gates by depleting the 2DHG underneath. The additional global top Gate, TG_{Global} in sample **A** increases the device tunability.

In order to characterize the sample and show the large phase space available, we use sample **B** to individually tune two SQDs before demonstrating how the center barrier determines the tunnel coupling between these two dots. Fig. 2(a) shows Coulomb diamonds of the left SQD formed on the left side by leaving the gates RB and PLR unused, i.e. at a constant voltage similar to the one applied to TG . On the other hand, Fig. 2(b) displays Coulomb diamonds of the right SQD formed with gates LB and PLL unused. From the Coulomb diamonds, we determine lever arms $\alpha_L = 0.22 \text{ eV/V}$ and $\alpha_R = 0.26 \text{ eV/V}$, for the left and

right SQD, respectively, and extract an electron temperature of $T = 50$ mK from the width of a low-bias Coulomb peak measured in the right dot. The charging energy $E_C = 1.2$ mV yields an estimate for the dot radius,³⁵ $r \approx \frac{e^2}{8\epsilon_0\epsilon E_C} = 117$ nm, which fits the lithographic width of the SQD. In the estimate, we used the electron charge, e , and permittivities ϵ_0 in vacuum and $\epsilon = 16.2$ in Ge.³⁶ In both SQDs we observe excited states with typical excitation energies on the order of $\Delta = 150$ μ eV, which is as well within the regime expected from a simple harmonic oscillator model and using the extracted dot-radius and the light hole effective mass $m^* = 0.09 m_e$ measured in a similar 2DHG.¹⁶

We continue to form a DQD by using the left (*LB*) and right (*RB*) barrier gates to tune the coupling to the respective leads and *CB* to tune the tunnel coupling in-between the two SQDs. Starting with $V_{CB} = 0.56$ V, the large inter-dot tunnel coupling hybridizes the two SQDs to a molecule and leads to the charge stability diagram displayed in Fig. 2(c). There, the current flows through the device whenever the electrochemical potential of the hybridized quantum dot molecule lies between the source and the drain electrochemical potentials. Upon lowering the inter-dot tunnel coupling by increasing V_{CB} , the two dots are being decoupled and the areas where current flows is continuously restricted to the triple points,³⁷ see Fig. 2(d-f). To estimate the change in tunneling conductance, we follow the discussions in Refs. 35,37,38 which conclude that the energies of the individual states can be resolved if the tunneling conductance is smaller than e^2/h , where h is the Heisenberg constant. Hence, in the most conductive regime, where we do not resolve individual SQD states, the interdot tunneling conductance is larger than e^2/h , while it must be much smaller than e^2/h in order to dominate the transport in the least conductive regimes.

Pauli spin blockade and charge sensing

The read-out of a future S - T_0 -qubit relies on the PSB^{24,39} for spin-to-charge conversion and a charge readout scheme. We will first address the PSB in Fig. 3(a-c) before going into detail of charge sensing below. In the experiment, PSB is characterized by a suppression of current

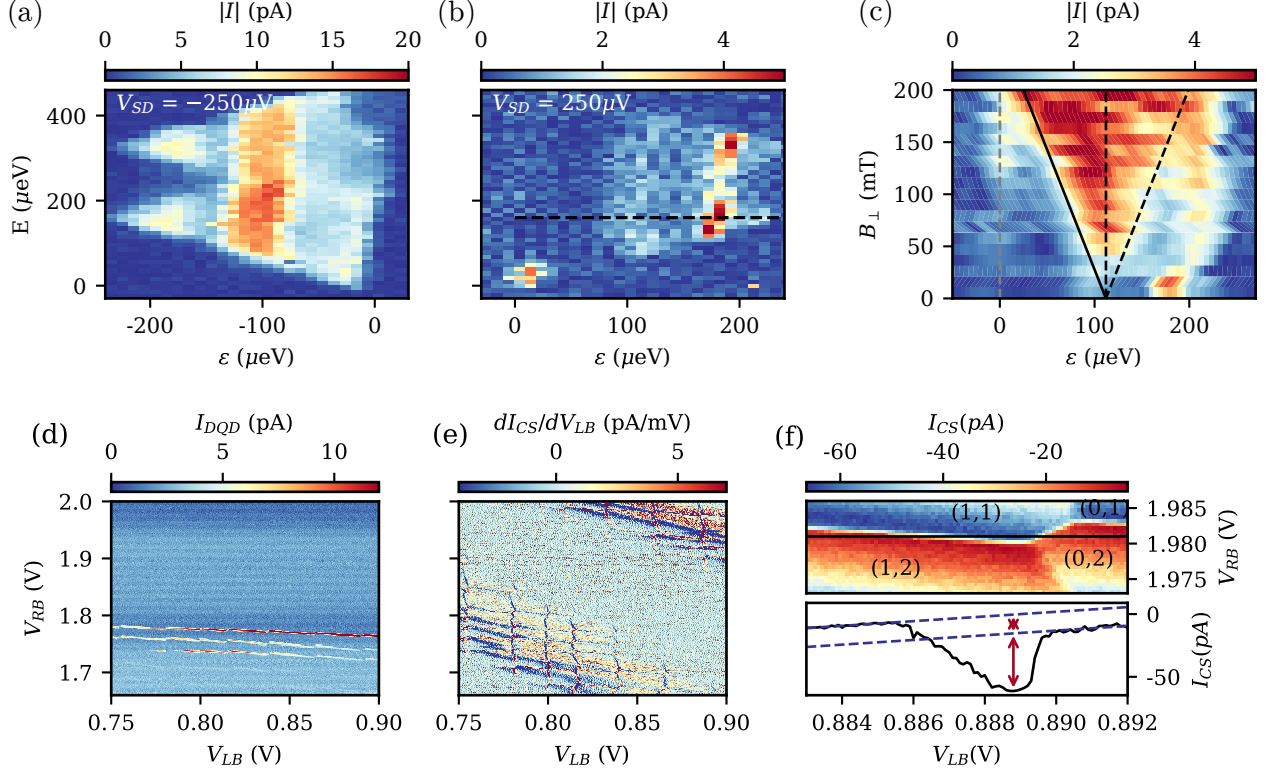


Figure 3: Spin blockade and charge readout. Panels (a-c) show the PSB and panels (d-f) refer to the charge readout scheme. The absolute value of the current through the DQD is shown for $V_{SD} = -250 \mu\text{V}$ in panel (a) and $V_{SD} = 250 \mu\text{V}$ in panel (b), both measured at $B_{\perp} = 21 \text{ mT}$. In (b), the signal is weak along the inter-dot line and enhanced when current starts to flow through the $(0, 2)$ triplet state. We repeat these measurements for various values of B_{\perp} , extract traces as indicated by the black dashed line in (b) for each value of the magnetic field and plot them in panel (c). The dashed grey line indicates zero detuning and the black lines follow the position of the $(0, 2)$ triplet states, solid for T_{+} and dashed for T_{0} and T_{-} . Panels (d) and (e) display the current through the DQD and transconductance of charge sensor dot, respectively. Changes in charge states of the DQD yield the hexagonal pattern observed in the sensor dot. The Coulomb blockade effect in the sensor dot modulates its sensitivity. A zoom-in of the charge detector current is shown in panel (f, top) together with a line-trace as indicated in black (bottom). Red arrows denote the jumps of differing amplitudes occurring due to electrons tunneling between different charge states of the DQD.

flow through the baseline of the bias triangles in forward bias direction, see Fig. 3(b), while current is allowed to flow in the reversed direction, as shown in panel (a). Here, forward denotes charge tunnelling through the DQD charge states $(0, 1) \rightarrow (1, 1) \rightarrow (0, 2) \rightarrow (0, 1)$, where (N_L, N_R) indicates a state with N_L holes in the left and N_R holes in the right dot, where zero is measured from an unknown offset. Then, spin blockade occurs when both,

the (1, 1) singlet and triplet states are available for transport, while for the (0, 2) state, only the singlet ground state is accessible. The blockade is lifted when the detuning equals the (0, 2) triplet excitation energy, defined by the orbital level spacing minus the difference in Coulomb energies.²¹ The resulting singlet-triplet splitting Δ_{ST} is readily extracted from the onset of current flow in the triangle displayed in Fig. 3(b), amounting to $\Delta_{ST} = 0.1$ meV in this case.

Applying a magnetic field perpendicular to the plane of the 2DHG, $B_{\perp} > 0$, the (0, 2) triplet states split with the spin-polarized triplet (T_{+}) state energy decreasing. For small enough magnetic field values where the cyclotron energy $\hbar|e|B_{\perp}/m^{*} = 16B_{\perp}$ meV is smaller than the confinement energy (of the order $\hbar^2/m^{*}(25\text{ nm})^2 = 0.1$ eV), we neglect orbital effects in order to approximate $\Delta_{ST}(B_{\perp}) = \Delta_{ST}(B_{\perp} = 0) - g_{\perp}\mu_B B_{\perp}$. This allows us to extract a first estimate of the out-of plane g -factor, as we show in Fig. 3(c). There, we plot in black the line defining $\Delta_{ST}(B_{\perp})$ with $g_{\perp} = 7.5$. We will return to discussing g -factors in more detail below. Additionally, in Fig. 3(c), we indicate in black dashed lines how the two remaining triplet states (T_0 and T_{-}) evolve with magnetic field.

We now turn to the charge readout mechanism, which relies on the capacitive coupling of the DQD under study to a charge-sensitive conductor.^{21,40} Here, we use sample **A** with a DQD gate layout similar to sample **B** but with the addition of a SQD in close vicinity to it, see Fig. 1(b). The current through the additional charge sensor dot, I_{CS} , exhibits steps whenever the electronic configuration of the DQD is changed. Fig. 3 shows the current I_{DQD} measured through the DQD in panel (d) and the numerical dI_{CS}/dV_{LB} through the sensor dot in panel (e), recorded in the same measurement. While the signal I_{DQD} vanishes in the noise background, the transconductance through the charge sensor dot maps the DQD's hexagonal charge stability diagram. The modulation of the signal intensity is caused by Coulomb oscillations in the sensor dot.

A zoom-in of I_{CS} is provided in Fig. 3(f,top), together with a trace along the line indicated in black (bottom). The step-height of I_{CS} occurring due to charge transitions in the DQD

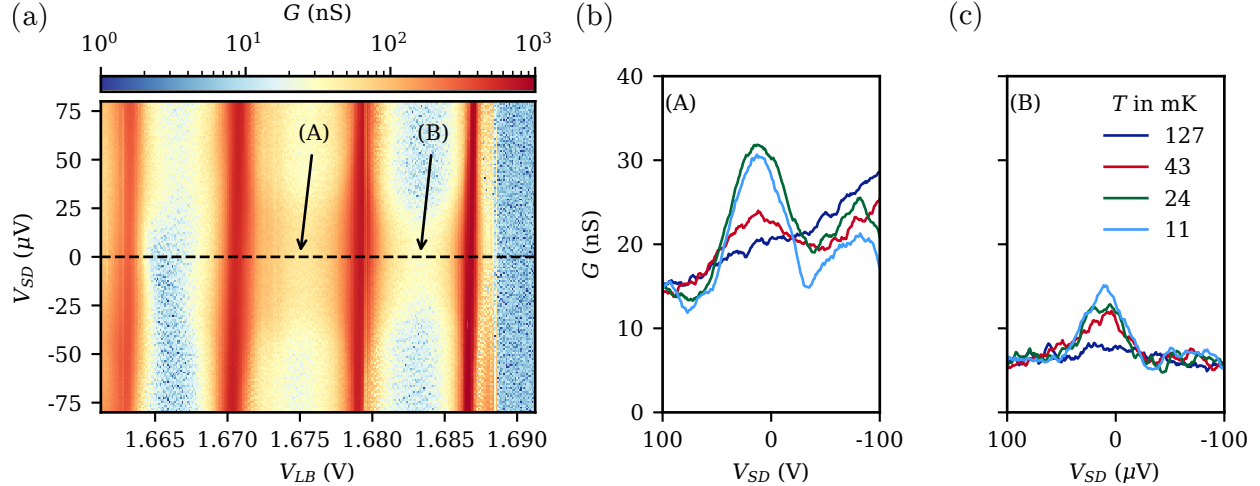


Figure 4: The Kondo effect. The measured (using standard lock-in techniques) conductance as a function of gate and bias voltage, displayed in (a), exhibits peaks and valleys not only as expected due to the Coulomb blockade effect but also in-between Coulomb peaks. The additional peaks are labelled (A) and (B) and are studied as a function of temperature in panels (b) and (c), respectively. Their decay with temperature suggests Kondo temperatures smaller than 127 mK.

depends on the involved charge states. In particular, we clearly distinguish the inter-dot transition $(0, 2) - (1, 1)$ from the transition $(1, 2) - (1, 1)$ where an electron is exchanged with a reservoir. Together with the PSB demonstrated above, this fulfills the requirement of a spin-readout mechanism.

***g*-factor anisotropy**

The all-electrical control of a S - T_0 -qubit requires different g -factors in the two SQDs forming the DQD. It is therefore interesting to study in detail the g -factors, which we do in the following via measuring the splitting of a Kondo peak in an applied magnetic field.

In a first step, we tune the left SQD of device **B** into a regime where at least one barrier is transparent enough to observe the Kondo effect.⁴¹ Fig. 4(a) displays the conductance G at low bias and varying gate-voltage. It peaks due to Coulomb resonances, and additionally, two regions labeled (A) and (B) exhibit increased conductance at $V_{SD} = 0$. Fig 4(b) and (c) show line-traces through the conductance peaks (A) and (B), respectively, at fixed gate voltages

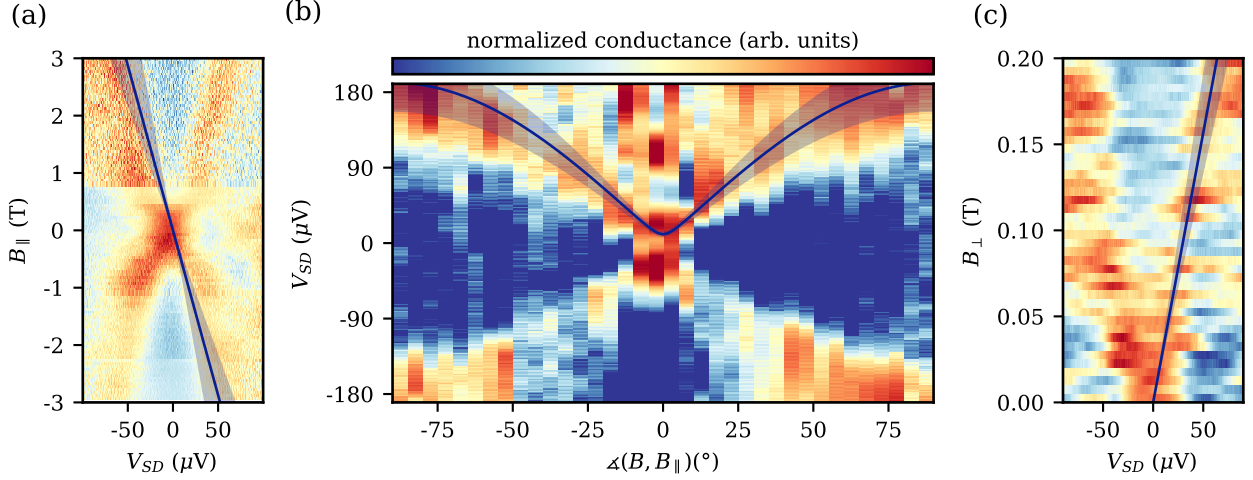


Figure 5: g -factor anisotropy. The conductance is shown as a function of in-plane field in (a), as a function of out-of-plane field in (c) and as a function of out-of-plane angle (at $|B| = 0.6$ T) in (b). The conductance was measured with standard lock-in techniques and the values measured at different angles have been normalized to a common minimum and maximum. The blue lines display the condition $|e|V_{SD} = g\mu_B B$ for the g -factors $g_{\parallel} = 0.3$ and $g_{\perp} = 5.5$. The error bars define the boundaries of the blue shaded regions.

and varying temperatures. As expected for the Kondo effect, the conductance decreases for increasing temperature and vanishes above the Kondo temperature T_K . From the full width at half maximum of the conductance peak (A) at the lowest temperature, we estimate $T_K = 100$ mK. The occurrence of Kondo peaks in two consecutive Coulomb-valleys likely results from orbital degeneracies in the quantum dot energy spectrum, similar as observed in Ref. 42.

We go on to extract the g -factors in and out-of plane by using the splitting of peak (A) in an applied magnetic field. With the field parallel to the plane of the 2DHG, the splitting is characterized by g_{\parallel} , as shown in Fig. 5(a). Similarly, again neglecting orbital effects, Fig. 5(c) shows the splitting of the conductance peak due g_{\perp} and an applied magnetic field perpendicular to the 2DHG-plane. The g -factors extracted from the inflection points of the conductance⁴³ as measured in panels (a) and (c) are $g_{\perp} = 5.5 \pm 1.0$ and $g_{\parallel} = 0.3 \pm 0.1$, respectively, which we plot in blue lines within shaded regions corresponding to the error bars. Finally, we fix the amplitude of the magnetic field at $|B| = 0.6$ T and measure the conductance as a function of the out-of plane angle. The anisotropy of the g -factor is visible in

the resulting measurement, Fig. 5(b). Following Refs. 44,45 we write $g(B_{\parallel}, B_{\perp}) = \frac{\sqrt{g_{\parallel}^2 B_{\parallel}^2 + g_{\perp}^2 B_{\perp}^2}}{\sqrt{B_{\parallel}^2 + B_{\perp}^2}}$ for the two-dimensional case at hand. Correspondingly, we indicate in panel (b) using a blue line and a shaded region the behavior of the conductance peaks expected by plugging in the g_{\parallel} and g_{\perp} measured as described above. This measurement at constant field underestimates the value for g_{\perp} probably due to orbital effects starting to play a role at $|B| = 0.6$ T.

The measured value of g_{\perp} is smaller than the theoretically predicted value $g_{\perp} = 21.4$ for pure heavy-hole states.⁴⁶ Admixture of light hole states due the confinement into zero dimensions or strain generally reduces the g -factor.⁸ However, calculations for hut-wires¹⁰ show that the confinement alone does not reduce the heavy-hole character by more than 1%. More likely, leakage of the confined states into the SiGe barriers causes the reduction, as $g = 2$ for holes in Si.⁴⁷

The anisotropy of the g -factor brings about an interesting tuning knob for a S - T_0 -qubit.³⁰ For the rotation along the qubit axis, we rely on a difference in g -factors between the left and right SQD. It has been shown²⁴ that small differences in the percentage range can be achieved. Extrapolating from this, we propose to use the shown anisotropy to chose the absolute value of g and hence, expecting a similar percentage range of tunability, its difference in the two SQDs.

Conclusion

We conclude that Ge/SiGe heterostructures possess all the necessary ingredients for building an all-electrically tunable S - T_0 -qubit. A qubit can readily be encoded in the singlet and unpolarized triplet states of a DQD built from two individually tunable SQDs. Readout of the qubit will occur through charge sensing and the PSB regime. The rotation along the equator may be tuned by the tunnel-coupling between the dots. For the rotation along the qubit axis we can chose the value of the g -factor by correspondingly aligning the magnetic field. Apart from choosing a path towards quantum computing with quantum dots, the large

g -factors together with the elsewhere demonstrated coupling to superconductors^{48,49} and long ballistic one-dimensional channels⁵⁰ make Ge/SiGe an interesting material for studying topologically protected states.^{51,52}

Fabrication of the devices

A 90 s long etching process in an SF₆-O₂-CHF₃ reactive ion plasma leaves a mesa on the heterostructure. The etch depth amounts to ≈ 70 nm. Electric contacts to the Ge consist of a 60 nm thick layer of Pt deposited after removing the native oxide with an in-situ Ar milling process (2×2 min at 10 mA and 300 V) in the same machine and without breaking the vacuum. These contacts are covered with 200 cycles (≈ 20 nm) of thermal aluminium oxide grown in an ALD at 300 °C. The depletion gates consist of 3 nm Ti and 92 nm Pd. A second layer of the same oxide isolates the depletion gates from the accumulation gates, which consist of 3 nm Ti and 102 nm Pd. The patterns for all layers are defined using electron-beam lithography at 100 keV.

Acknowledgement

We thank Matthias Brauns for helpful discussions and careful proofreading of the manuscript. This project has received funding from the European Union's Horizon 2020 research and innovation program under the Marie Skłodowska-Curie grant agreement No 844511 and from the FWF project P30207. The research was supported by the Scientific Service Units of IST Austria through resources provided by the MIBA machine shop and the nanofabrication facility.

Note

While writing this manuscript, we became aware of an experiment⁵³ where a Ge quantum dot based on a similar heterostructure as the one used in this study shows charge sensing of a quantum dot filled to the last hole.

References

- (1) Lu, W.; Xiang, J.; Timko, B. P.; Wu, Y.; Lieber, C. M. One-dimensional hole gas in germanium/silicon nanowire heterostructures. *Proceedings of the National Academy of Sciences* **2005**, *102*, 10046–10051.
- (2) Roddaro, S.; Fuhrer, A.; Brusheim, P.; Fasth, C.; Xu, H. Q.; Samuelson, L.; Xiang, J.; Lieber, C. M. Spin States of Holes in Ge / Si Nanowire Quantum Dots. *Physical Review Letters* **2008**, *101*, 186802.
- (3) Hu, Y.; Kuemmeth, F.; Lieber, C. M.; Marcus, C. M. Hole spin relaxation in Ge-Si core-shell nanowire qubits. *Nature Nanotechnology* **2012**, *7*, 47–50.
- (4) Higginbotham, A.; Kuemmeth, F.; Larsen, T.; Fitzpatrick, M.; Yao, J.; Yan, H.; Lieber, C.; Marcus, C. Antilocalization of Coulomb Blockade in a Ge/Si Nanowire. *Physical Review Letters* **2014**, *112*, 216806.
- (5) Brauns, M.; Ridderbos, J.; Li, A.; Bakkers, E. P. A. M.; Zwanenburg, F. A. Electric-field dependent g -factor anisotropy in Ge-Si core-shell nanowire quantum dots. *Physical Review B* **2016**, *93*, 121408.
- (6) Brauns, M.; Ridderbos, J.; Li, A.; Bakkers, E. P. A. M.; van der Wiel, W. G.; Zwanenburg, F. A. Anisotropic Pauli spin blockade in hole quantum dots. *Physical Review B* **2016**, *94*, 041411.

- (7) Katsaros, G.; Spathis, P.; Stoffel, M.; Fournel, F.; Mongillo, M.; Bouchiat, V.; Lefloch, F.; Rastelli, A.; Schmidt, O. G.; De Franceschi, S. Hybrid superconductor-semiconductor devices made from self-assembled SiGe nanocrystals on silicon. *Nature Nanotechnology* **2010**, *5*, 458–464.
- (8) Ares, N.; Golovach, V. N.; Katsaros, G.; Stoffel, M.; Fournel, F.; Glazman, L. I.; Schmidt, O. G.; De Franceschi, S. Nature of Tunable Hole g Factors in Quantum Dots. *Physical Review Letters* **2013**, *110*, 046602.
- (9) Zhang, J. J.; Katsaros, G.; Montalenti, F.; Scopece, D.; Rezaev, R. O.; Mickel, C.; Rellinghaus, B.; Miglio, L.; De Franceschi, S.; Rastelli, A.; Schmidt, O. G. Monolithic Growth of Ultrathin Ge Nanowires on Si(001). *Physical Review Letters* **2012**, *109*, 085502.
- (10) Watzinger, H.; Kloeffel, C.; Vukušić, L.; Rossell, M. D.; Sessi, V.; Kukučka, J.; Kirchschrager, R.; Lausecker, E.; Truhlar, A.; Glaser, M.; Rastelli, A.; Fuhrer, A.; Loss, D.; Katsaros, G. Heavy-Hole States in Germanium Hut Wires. *Nano Letters* **2016**, *16*, 6879–6885.
- (11) Watzinger, H.; Kukučka, J.; Vukušić, L.; Gao, F.; Wang, T.; Schäffler, F.; Zhang, J.-J.; Katsaros, G. A germanium hole spin qubit. *Nature Communications* **2018**, *9*, 3902.
- (12) Vukušić, L.; Kukučka, J.; Watzinger, H.; Katsaros, G. Fast Hole Tunneling Times in Germanium Hut Wires Probed by Single-Shot Reflectometry. *Nano Letters* **2017**, *17*, 5706–5710.
- (13) Vukušić, L.; Kukučka, J.; Watzinger, H.; Milem, J. M.; Schäffler, F.; Katsaros, G. Single-Shot Readout of Hole Spins in Ge. *Nano Letters* **2018**, *18*, 7141–7145.
- (14) Xu, G.; Li, Y.; Gao, F.; Li, H.-O.; Liu, H.; Wang, K.; Cao, G.; Xiao, M.; Wang, T.; Zhang, J.-J.; Guo, G.-C.; Guo, G.-P. Dipole coupling of a tunable hole double quantum dot in germanium hut wire to a microwave resonator. *arXiv:1905.01586* **2019**,

- (15) Dobbie, A.; Myronov, M.; Morris, R. J. H.; Hassan, A. H. A.; Prest, M. J.; Shah, V. A.; Parker, E. H. C.; Whall, T. E.; Leadley, D. R. Ultra-high hole mobility exceeding one million in a strained germanium quantum well. *Applied Physics Letters* **2012**, *101*, 172108.
- (16) Sammak, A.; Sabbagh, D.; Hendrickx, N. W.; Lodari, M.; Paquelet Wuetz, B.; Tosato, A.; Yeoh, L.; Bollani, M.; Virgilio, M.; Schubert, M. A.; Zaumseil, P.; Capellini, G.; Veldhorst, M.; Scappucci, G. Shallow and Undoped Germanium Quantum Wells: A Playground for Spin and Hybrid Quantum Technology. *Advanced Functional Materials* **2019**, *29*, 1807613.
- (17) Borselli, M. G.; Eng, K.; Croke, E. T.; Maune, B. M.; Huang, B.; Ross, R. S.; Kiselev, A. A.; Deelman, P. W.; Alvarado-Rodriguez, I.; Schmitz, A. E.; Sokolich, M.; Holabird, K. S.; Hazard, T. M.; Gyure, M. F.; Hunter, A. T. Pauli spin blockade in undoped Si/SiGe two-electron double quantum dots. *Applied Physics Letters* **2011**, *99*, 063109.
- (18) Loss, D.; DiVincenzo, D. P. Quantum computation with quantum dots. *Physical Review A* **1998**, *57*, 120–126.
- (19) Koppens, F. H. L.; Buizert, C.; Tielrooij, K. J.; Vink, I. T.; Nowack, K. C.; Meunier, T.; Kouwenhoven, L. P.; Vandersypen, L. M. K. Driven coherent oscillations of a single electron spin in a quantum dot. *Nature* **2006**, *442*, 766–771.
- (20) Nowack, K. C.; Shafiei, M.; Laforest, M.; Prawiroatmodjo, G. E. D. K.; Schreiber, L. R.; Reichl, C.; Wegscheider, W.; Vandersypen, L. M. K. Single-Shot Correlations and Two-Qubit Gate of Solid-State Spins. *Science* **2011**, *333*, 1269–1272.
- (21) Hanson, R.; Kouwenhoven, L. P.; Petta, J. R.; Tarucha, S.; Vandersypen, L. M. K. Spins in few-electron quantum dots. *Reviews of Modern Physics* **2007**, *79*, 1217–1265.

- (22) Lodari, M.; Tosato, A.; Sabbagh, D.; Schubert, M. A.; Capellini, G.; Sammak, A.; Veldhorst, M.; Scappucci, G. Light effective hole mass in undoped Ge/SiGe quantum wells. *Physical Review B* **2019**, *100*, 041304.
- (23) Hendrickx, N. W.; Franke, D. P.; Sammak, A.; Kouwenhoven, M.; Sabbagh, D.; Yeoh, L.; Li, R.; Tagliaferri, M. L. V.; Virgilio, M.; Capellini, G.; Scappucci, G.; Veldhorst, M. Gate-controlled quantum dots and superconductivity in planar germanium. *Nature Communications* **2018**, *9*, 2835.
- (24) Hendrickx, N. W.; Franke, D. P.; Sammak, A.; Scappucci, G.; Veldhorst, M. Fast two-qubit logic with holes in germanium. *arXiv:1904.11443* **2019**,
- (25) Fischer, J.; Coish, W. A.; Bulaev, D. V.; Loss, D. Spin decoherence of a heavy hole coupled to nuclear spins in a quantum dot. *Physical Review B* **2008**, *78*, 155329.
- (26) Testelin, C.; Bernardot, F.; Eble, B.; Chamarro, M. Hole spin dephasing time associated with hyperfine interaction in quantum dots. *Physical Review B* **2009**, *79*, 195440.
- (27) Petta, J. R. Coherent Manipulation of Coupled Electron Spins in Semiconductor Quantum Dots. *Science* **2005**, *309*, 2180–2184.
- (28) Levy, J. Universal Quantum Computation with Spin- 1/2 Pairs and Heisenberg Exchange. *Physical Review Letters* **2002**, *89*, 147902.
- (29) Foletti, S.; Bluhm, H.; Mahalu, D.; Umansky, V.; Yacoby, A. Universal quantum control of two-electron spin quantum bits using dynamic nuclear polarization. *Nature Physics* **2009**, *5*, 903–908.
- (30) Jock, R. M.; Jacobson, N. T.; Harvey-Collard, P.; Mounce, A. M.; Srinivasa, V.; Ward, D. R.; Anderson, J.; Manginell, R.; Wendt, J. R.; Rudolph, M.; Pluym, T.;

- Gamble, J. K.; Baczewski, A. D.; Witzel, W. M.; Carroll, M. S. A silicon metal-oxide-semiconductor electron spin-orbit qubit. *Nature Communications* **2018**, *9*, 1768.
- (31) Terrazos, L. A.; Marcellina, E.; Coppersmith, S. N.; Friesen, M.; Hamilton, A. R.; Hu, X.; Koiller, B.; Saraiva, A. L.; Culcer, D.; Capaz, R. B. Qubits Based on Hole Quantum Dots in Strained Ge. **2018**,
- (32) Morrison, C.; Wiśniewski, P.; Rhead, S. D.; Foronda, J.; Leadley, D. R.; Myronov, M. Observation of Rashba zero-field spin splitting in a strained germanium 2D hole gas. *Applied Physics Letters* **2014**, *105*, 182401.
- (33) Hardy, W. J.; Harris, C. T.; Su, Y.-H.; Chuang, Y.; Moussa, J.; Maurer, L. N.; Li, J.-Y.; Lu, T.-M.; Luhman, D. R. Single and double hole quantum dots in strained Ge/SiGe quantum wells. *Nanotechnology* **2019**, *30*, 215202.
- (34) Rössner, B.; Chrastina, D.; Isella, G.; von Känel, H. Scattering mechanisms in high-mobility strained Ge channels. *Applied Physics Letters* **2004**, *84*, 3058–3060.
- (35) Ihn, T. *Semiconductor Nanostructures*; Oxford University Press, 2009.
- (36) NSM@mail.ioffe.ru, Basic Parameters of Germanium (Ge). <http://www.ioffe.ru/SVA/NSM/Semicond/Ge/basic.html>.
- (37) Livermore, C.; Crouch, C. H.; Westervelt, R. M.; Campman, K. L.; Gossard, A. C. The Coulomb Blockade in Coupled Quantum Dots. *Science (New York, N.Y.)* **1996**, *274*, 1332–5.
- (38) Matveev, K. A.; Glazman, L. I.; Baranger, H. U. Coulomb blockade of tunneling through a double quantum dot. *Physical Review B* **1996**, *54*, 5637–5646.
- (39) Ono, K.; Austing, D. G.; Tokura, Y.; Tarucha, S. Current rectification by Pauli exclusion in a weakly coupled double quantum dot system. *Science (New York, N.Y.)* **2002**, *297*, 1313–7.

- (40) Field, M.; Smith, C. G.; Pepper, M.; Ritchie, D. A.; Frost, J. E. F.; Jones, G. A. C.; Hasko, D. G. Measurements of Coulomb blockade with a noninvasive voltage probe. *Physical Review Letters* **1993**, *70*, 1311–1314.
- (41) Franceschi, S. D.; van der Wiel, W. G. In *Handbook of Nanophysics: Nanoparticles and Quantum Dots*; Sattler, K. D., Ed.; CRC Press, 2010; Chapter Kondo Effect, pp 646–664.
- (42) Li, R.; Hudson, F. E.; Dzurak, A. S.; Hamilton, A. R. Pauli Spin Blockade of Heavy Holes in a Silicon Double Quantum Dot. *Nano Letters* **2015**, *15*, 7314–7318.
- (43) Csonka, S.; Hofstetter, L.; Freitag, F.; Oberholzer, S.; Schönenberger, C.; Jespersen, T. S.; Aagesen, M.; Nygård, J. Giant Fluctuations and Gate Control of the g -Factor in InAs Nanowire Quantum Dots. *Nano Letters* **2008**, *8*, 3932–3935.
- (44) Petta, J. R.; Ralph, D. C. Measurements of Strongly Anisotropic g Factors for Spins in Single Quantum States. *Physical Review Letters* **2002**, *89*, 156802.
- (45) Brouwer, P. W.; Waintal, X.; Halperin, B. I. Fluctuating Spin g -Tensor in Small Metal Grains. *Physical Review Letters* **2000**, *85*, 369–372.
- (46) van Kesteren, H. W.; Cosman, E. C.; van der Poel, W. A. J. A.; Foxon, C. T. Fine structure of excitons in type-II GaAs/AlAs quantum wells. *Physical Review B* **1990**, *41*, 5283–5292.
- (47) Voisin, B.; Maurand, R.; Barraud, S.; Vinet, M.; Jehl, X.; Sanquer, M.; Renard, J.; De Franceschi, S. Electrical Control of g -Factor in a Few-Hole Silicon Nanowire MOSFET. *Nano Letters* **2016**, *16*, 88–92.
- (48) Vigneau, F.; Mizokuchi, R.; Zanuz, D. C.; Huang, X.; Tan, S.; Maurand, R.; Frolov, S.; Sammak, A.; Scappucci, G.; Lefloch, F.; De Franceschi, S. Germanium Quantum-Well Josephson Field-Effect Transistors and Interferometers. *Nano Letters* **2019**, *19*, 1023–1027.

- (49) Hendrickx, N. W.; Tagliaferri, M. L. V.; Kouwenhoven, M.; Li, R.; Franke, D. P.; Sammak, A.; Brinkman, A.; Scappucci, G.; Veldhorst, M. Ballistic supercurrent discretization and micrometer-long Josephson coupling in germanium. *Physical Review B* **2019**, *99*, 075435.
- (50) Mizokuchi, R.; Maurand, R.; Vigneau, F.; Myronov, M.; De Franceschi, S. Ballistic One-Dimensional Holes with Strong g-Factor Anisotropy in Germanium. *Nano Letters* **2018**, *18*, 4861–4865.
- (51) Lutchyn, R. M.; Sau, J. D.; Das Sarma, S. Majorana Fermions and a Topological Phase Transition in Semiconductor-Superconductor Heterostructures. *Physical Review Letters* **2010**, *105*, 077001.
- (52) Oreg, Y.; Refael, G.; von Oppen, F. Helical Liquids and Majorana Bound States in Quantum Wires. *Physical Review Letters* **2010**, *105*, 177002.
- (53) Lawrie, W. I. L. et al. Quantum Dot Arrays in Silicon and Germanium. *arXiv:1909.06575* **2019**,